

# Efficient method for estimating the dynamics of the full polarizability tensor during *ab initio* molecular dynamics simulations

Pouya Partovi-Azar \*

*Institute of Chemistry, Martin Luther University Halle-Wittenberg, Von-Danckelmann-Platz 4, 06120 Halle (Saale), Germany*

 (Received 6 November 2023; revised 4 December 2023; accepted 5 December 2023; published 19 December 2023)

An efficient method is presented to approximate the dynamics of individual polarizability tensor elements, for example, during *ab initio* molecular dynamics simulations. The method is based on the calculation of the quadrupole moment matrix of the position operator in the maximally localized Wannier functions representation. The presented method has a wide range of applications, particularly in vibrational spectroscopy simulations, such as (resonance) Raman, Raman optical activity, sum-frequency generation, etc. It is demonstrated that this method can lead to a several-hundred-times speedup with respect to reference linear response calculations. The predictive power of the introduced method is tested in the cases of various molecules as well as depolarized Raman spectra of gaseous and liquid methanol, in all of which remarkable agreement with the reference spectra is observed.

DOI: [10.1103/PhysRevB.108.235157](https://doi.org/10.1103/PhysRevB.108.235157)

## I. INTRODUCTION

Electric polarizability is one of the fundamental properties of materials and describes the tendency of a material to change its dipole moment upon being subject to an external electric field. Evolution of the electric polarizability of a material during a certain process provides invaluable information about many of its chemical and physical properties. Therefore estimation of the full polarizability tensor lies at the heart of many spectroscopy simulations, for example, polarized and depolarized Raman, Raman optical activity, sum-frequency generation, etc. [1–7]

Despite promising methods devised in the past decade to facilitate computation of vibrational spectra based on *ab initio* molecular dynamics (AIMD) simulations, application of such methods has been limited to small systems and fast processes [7]. This is, partly, due to the huge computational cost of such simulations, especially in cases where the full polarizability tensor of a system is needed [8,9]. The calculation of the polarizability tensor could, in fact, be an order of magnitude more costly than generating the trajectory itself.

Nevertheless, it has been shown that in the case of Raman spectroscopy simulations, a substantial speedup can be achieved by using the Wannier polarizability (WP) method, which allows for on-the-fly calculation of the mean polarizability of a system during an AIMD simulation, avoiding a direct computation of the full polarizability tensor through the finite-difference method or linear response (LR) theory [10,11]. However, the applicability of the WP method is limited to the simulation of polarized Raman spectra, where only the mean polarizability is required, and therefore linear response theory [12–17] and the finite-difference scheme [5,6,18] have remained the methods of choice for simulating, for example, depolarized Raman and sum-frequency generation spectra.

In this paper, an efficient method is introduced to extend applicability of the WP method to spectroscopy simulations where the full polarizability tensor is required. The aim is set at reproducing the correct dynamics of the static polarizability tensor during AIMD simulations. This is achieved by calculating the quadrupole moment matrix of the position operator in the maximally localized Wannier functions representation and gives a substantial speedup over calculations using linear response theory or the finite-difference method. The predictive power of this method is checked against reference linear response calculations in the cases of various molecules and clusters as well as liquid methanol.

## II. METHODOLOGY

### A. Covariance matrix of the position operator in the Wannier representation

Maximally localized Wannier functions (MLWFs) [19,20] allow for partitioning the total electronic charge distribution in a system into fragment contributions. They are defined as

$$w_n(\mathbf{r} - \mathbf{R}) = \frac{V}{(2\pi)^3} \int_{\text{BZ}} d\mathbf{k} e^{-i\mathbf{k}\cdot\mathbf{r}} \sum_{m=1}^J U_{mn}^{(\mathbf{k})} \psi_{m\mathbf{k}}(\mathbf{r}). \quad (1)$$

Here,  $\psi_{m\mathbf{k}}(\mathbf{r})$  are Bloch eigenstates as obtained from an electronic structure method, such as density functional theory (DFT) [21],  $\mathbf{R}$  is a Bravais lattice vector,  $V$  is the real-space primitive cell volume, and the integral is computed over the whole Brillouin zone (BZ). To compute MLWFs, the functional

$$Q_{\text{tot}} = \sum_n^{N_{\text{WF}}} Q_n = \sum_n^{N_{\text{WF}}} [\langle w_n | r^2 | w_n \rangle - \langle w_n | \mathbf{r} | w_n \rangle^2] \quad (2)$$

is minimized by appropriately chosen unitary rotations  $U_{mn}^{(\mathbf{k})}$  [22–24]. With minimized  $Q_{\text{tot}}$ , the isotropic extension of the

\*pouya.partovi-azar@chemie.uni-halle.de

Wannier function  $n$  can be then obtained by  $S_n = Q_n^{1/2}$ , which has units of length.

In the Wannier polarizability (WP) method [10,11] the mean polarizability is directly calculated based on MLWF spreads as

$$\bar{A} = \frac{\beta}{3} \sum_n^{N_{WF}} S_n^3, \quad (3)$$

with  $\beta$  being a constant. As such, the mean polarizability is calculated without a need for calculating individual elements of the polarizability tensor. The WP method has been successfully employed for simulating *ab initio* polarized Raman spectra of various systems with only a minimal extra computational cost required for the calculation of MLWFs [10,11,25–27].

The WP method directly connects the mean polarizability to the volume of electronic fragments in the system, inspired by the fact that the polarizability of molecules is known to be, to a first approximation, linearly proportional to their volume [28–31]. Following a similar line of thought, here we propose a direct relation between the individual elements of the polarizability tensor and the spatial extent of electronic fragments (MLWFs) along different directions. To this end, the quadrupole moment matrix of the position operator in the MLWFs representation is used.

To calculate the quadrupole moment matrix, one can adapt the approach of Wheeler *et al.* [32] and Kang *et al.* [33], which, extending the original work by Resta (which enables one to calculate the polarization of a many-body ground state [34]), allows for the calculation of the quadrupole moment (covariance) matrix based on periodic operators for  $pq$ , with  $p, q \in \{x, y, z\}$ . In this paper, however, nonperiodic operators for  $x, y$ , and  $z$  components are employed to define a  $3 \times 3$  covariance matrix for each Wannier function  $w_n$  as

$$c_{n,pq} = [\langle w_n | pq | w_n \rangle - \langle w_n | p | w_n \rangle \langle w_n | q | w_n \rangle]^{\frac{1}{2}}, \quad (4)$$

where  $p, q \in \{x, y, z\}$  and  $\langle w_n | p | w_n \rangle$  is the  $p$  component of the Wannier center. It is observed that the computation of covariance matrices using nonperiodic operators is much faster than computations based on periodic position operators. The spread of each MLWF is related to the trace of its covariance matrix as

$$S_n = \text{Tr}[c_n]. \quad (5)$$

We define the total covariance matrix for the whole system as

$$\mathbf{\Omega} = \left( \sum_{i=1}^{N_{WF}} c_i \right)^3. \quad (6)$$

In Eq. (6),  $\mathbf{\Omega}$  is a symmetric  $3 \times 3$  matrix, and the third power, similar to Eq. (3), ensures the same physical units as  $A$ .

It is, in principle, possible to present a direct relation between  $\mathbf{\Omega}$  and  $A$  by introducing a proportionality constant [such as  $\beta$  in Eq. (3)]. Such a constant would generally be system dependent, in which case a single-point reference calculation (for example, using LR theory) would be enough to estimate it by comparing  $\mathbf{\Omega}$  with  $A$  for the system under study. The obtained value for the proportionality constant could then be used throughout an AIMD simulation (see below). However,

here the aim is not to estimate the polarizability tensor  $A$  with a high accuracy; rather, the goal is to approximate the dynamics of its individual elements during AIMD simulations based on those of the total covariant matrix  $\mathbf{\Omega}$ . Since the time series [such as  $A_{pq}(t)$  and  $\Omega_{pq}(t)$ ] should be normalized in the autocorrelation formalism for simulating finite-temperature spectra (see below), introducing such a proportionality constant is not necessary for spectroscopy simulations.

Equation (6) incorporates the cross terms between covariance matrices of different Wannier centers into  $\mathbf{\Omega}$ . Such terms are neglected in Eq. (3) for the mean polarizability. The effect of cross correlations between local physical quantities has already been shown to be crucial in spectroscopy simulations [1,3,4]. In the original WP method, neglecting such effects could result in inaccurate relative Raman intensities, where the total spectra are primarily dominated by Wannier functions with larger volumes [35].

Finally, it is observed that, even in the case of extended systems where the Wannier center does not constantly fluctuate between the neighboring unit cells, the approximate dynamics of the polarizability tensor calculated through Eq. (6) using nonperiodic position operators results in vibrational spectra which agree very well with reference linear response spectra (see below).

## B. Polarized and depolarized Raman intensities

The performance of the method introduced above is demonstrated in the case of finite-temperature depolarized Raman simulations. The total Raman intensity is given by [1,2,36]

$$I^{\text{Raman}} = I_{\text{pol}}^{\text{Raman}} + \frac{7}{30} I_{\text{depol}}^{\text{Raman}}. \quad (7)$$

The polarized and depolarized Raman intensities can be calculated through performing a Fourier transform of the polarizability autocorrelation function at thermodynamic equilibrium. This formalism fully takes the anharmonicity of the potential energy surface into account as the polarizability of the system is normally sampled throughout AIMD simulations at finite temperatures. The polarized and depolarized Raman intensities can be calculated using [2,4]

$$I_{\text{pol}}^{\text{Raman}} \propto C_{q/\text{cl}}(\nu) \int_{-\infty}^{\infty} dt e^{i2\pi\nu t} \langle \bar{A}(0) \bar{A}(t) \rangle_{\text{cl}},$$

$$I_{\text{depol}}^{\text{Raman}} \propto C_{q/\text{cl}}(\nu) \int_{-\infty}^{\infty} dt e^{i2\pi\nu t} \langle \text{Tr}[\mathbf{B}(0) \cdot \mathbf{B}(t)] \rangle_{\text{cl}}. \quad (8)$$

The mean polarizability  $\bar{A} = (A_{xx} + A_{yy} + A_{zz})/3$ , and  $C_{q/\text{cl}}(\nu) = \frac{h\nu/k_B T}{1 - \exp(-h\nu/k_B T)}$  is the quantum correction factor obtained based on harmonic approximation and has been shown to satisfy both the detailed balance condition and the fluctuation-dissipation theorem [37].  $\mathbf{B} = \mathbf{A} - \bar{A}\mathbf{I}$  represents the traceless anisotropic part of the polarizability tensor, with  $\mathbf{I}$  being the unity matrix, while  $\langle \dots \rangle_{\text{cl}}$  denotes the ensemble average of classical statistical mechanics. It can be shown that  $I_{\text{depol}}^{\text{Raman}} \sim \gamma^2 = \frac{1}{2} \sum_{p,q \in \{x,y,z\}} 3(A_{pq}A_{pq} - A_{pp}A_{qq})$ , where  $\gamma^2$  is the anisotropic Raman invariant [1,38]. As such, in the autocorrelation formalism, the depolarized Raman intensity

can be given by [5,13]

$$\begin{aligned}
I_{\text{depol}}^{\text{Raman}} \propto C_{\text{q/cl}}(\nu) & \left[ \int_{-\infty}^{\infty} dt e^{i2\pi\nu t} \langle [A_{xx}(0) - A_{yy}(0)] \right. \\
& \times [A_{xx}(t) - A_{yy}(t)]_{\text{cl}} \\
& + \int_{-\infty}^{\infty} dt e^{i2\pi\nu t} \langle [A_{xx}(0) - A_{zz}(0)] [A_{xx}(t) - A_{zz}(t)]_{\text{cl}} \\
& + \int_{-\infty}^{\infty} dt e^{i2\pi\nu t} \langle [A_{yy}(0) - A_{zz}(0)] [A_{yy}(t) - A_{zz}(t)]_{\text{cl}} \\
& + 6 \int_{-\infty}^{\infty} dt e^{i2\pi\nu t} \langle A_{xy}(0) A_{xy}(t) \rangle_{\text{cl}} \\
& + 6 \int_{-\infty}^{\infty} dt e^{i2\pi\nu t} \langle A_{xz}(0) A_{xz}(t) \rangle_{\text{cl}} \\
& \left. + 6 \int_{-\infty}^{\infty} dt e^{i2\pi\nu t} \langle A_{yz}(0) A_{yz}(t) \rangle_{\text{cl}} \right]. \quad (9)
\end{aligned}$$

### C. Computational details

All calculations are performed at the density functional theory (DFT) [21] level using the CP2K software package [39]. The DFT calculations are performed in conjunction with a TZVP-MOLOPT basis set (a basis set with triple-zeta valence plus one set of polarization functions optimized from molecular calculations) [40] as well as the Becke–Lee–Yang–Parr (BLYP) [41,42] exchange–correlation energy functional and Goedecker–Teter–Hutter (GTH) pseudopotentials [43,44]. The semiempirical DFT-with-dispersion-correction method DFT-D3 [45] is used to correct for the long-range dispersion interactions.

The maximum atomic force component used for structural optimization of molecules is 0.02 eV/Å. Structures of water clusters from the Cambridge Cluster Database are used without further optimization. The localization criterion for the total spread for the calculation of the MLWF through unitary Jacobi rotations is set to  $10^{-7}$ , whereas the target accuracy for the convergence of the conjugate gradient scheme in the reference linear response calculations of polarizability tensors is  $10^{-6}$ . MLWFs are first obtained using the Berry approach and are then used for the calculation of the covariance matrices according to Eq. (4).

All Raman spectra are obtained by performing 20-ps DFT-based AIMD simulations in the canonical ensemble to achieve equilibrium at 300 K, followed by 100-ps AIMD simulations in the microcanonical ensemble to remove thermostat effects and sample polarizabilities and Wannier functions. The temperature is controlled by a canonical sampling through velocity rescaling (CSVR) thermostat [46]. A time step of 1 fs is used in these simulations, and polarizabilities are sampled at each time step together with MLWFs. To simulate liquid methanol, a cubic unit cell of size  $15.00 \times 15.00 \times 15.00 \text{ \AA}^3$  containing 50 methanol molecules is used.

The linear response and Wannier localization modules have different parallel implementations in the CP2K software package. Therefore comparisons between the time needed for calculation of polarizability tensors using linear response theory,  $t_{\text{LR}}$ , and that required for obtaining total covariance matrices,  $t_{\text{WP}}$ , are made based on the speedup in latency,

TABLE I. Pearson correlation coefficient between elements of  $\Omega$  and  $A$ .

Coefficient	Correlation
$\rho(\Omega_{xx}, A_{xx})$	0.86
$\rho(\Omega_{yy}, A_{yy})$	0.80
$\rho(\Omega_{zz}, A_{zz})$	0.91
$\rho(\Omega_{xy}, A_{xy})$	0.63
$\rho(\Omega_{xz}, A_{xz})$	0.89
$\rho(\Omega_{yz}, A_{yz})$	0.96
$\rho(\text{Tr}[\Omega], \text{Tr}[A])$	0.86
$\rho(\gamma_{\Omega}^2, \gamma_A^2)$	0.84

$f = t_{\text{LR}}/t_{\text{WP}}$ , of single-core computations [35]. Here,  $t_{\text{WP}}$  includes both the time needed for obtaining MLWFs and that needed for computing the covariance matrices.

## III. RESULTS AND DISCUSSION

### A. Total covariance matrix

The total covariance matrix is calculated using Eq. (6) for a set of molecular structures consisting of nonpolar, polar, and charged conformations shown in Fig. 1(a). The aim here is to study the correlation between the total covariance matrix elements,  $\Omega_{pq}$ , in each structure and the corresponding elements of the reference polarizability tensor,  $A_{pq}$ , calculated using linear response (LR) theory. This is done by computing the Pearson correlation coefficients,  $\rho$ , which are given in Table I. In the calculation of correlations, the order of molecular systems is as shown in Fig. 1(a) (left to right, top to bottom). The correlation between the individual elements of  $A$  and  $\Omega$  is observed to be very strong, implying that the dynamics of the polarizability tensor,  $A$ , can reliably be approximated by that of the total covariance matrix,  $\Omega$ . However, computation of the total covariance matrices is found to be hugely less demanding computationally. The speedup, defined as the time needed for the calculation of polarizability tensors through LR theory with respect to that required for the calculation of total covariance matrices using the WP method for the same systems, is presented in Fig. 1(b) for the water clusters  $(\text{H}_2\text{O})_k$ ,  $k = 5, \dots, 20$ , shown in Fig. 1(a). In all clusters, the speedup is observed to be above 50 times. Even in the case of a bulk water sample consisting of 32 water molecules [shown as a solid square in Fig. 1(b)], a speedup of above 61 times is seen. Such a substantial speedup, as will be demonstrated below, is particularly beneficial for simulations of finite-temperature spectra through long AIMD trajectories. Figure 1(c) shows  $t_{\text{LR}}$  and  $t_{\text{WP}}$  for the same systems as functions of the number of electrons. It appears from the fits that substantial speedups could also be expected for larger systems containing similar molecules.

The main reason behind the observed speedup in the WP calculations has to do with the fact that the perturbed orbitals have to be computed iteratively in each LR calculation and their orthogonality condition has to be imposed. For the calculation of polarizability, this has to be repeated for three perturbative external electric fields along the  $x$ ,  $y$ , and  $z$  axes. Such calculations amount to a considerable computational cost (especially during AIMD simulations) which depends on the unit cell size, the fineness of the real-space grid, and

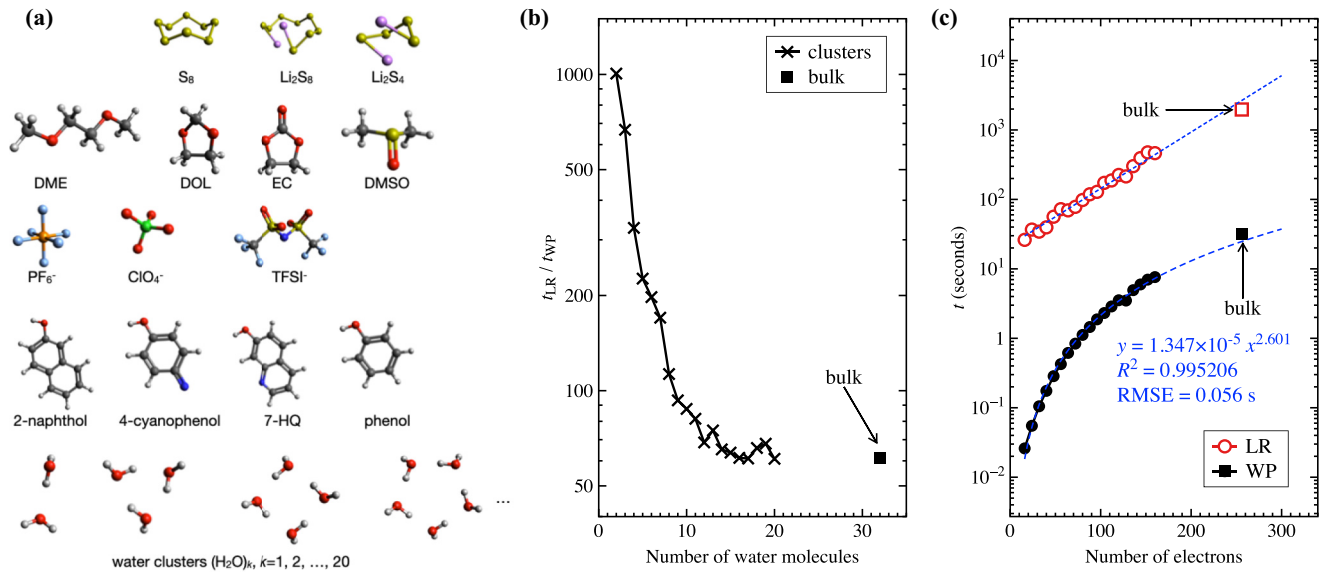


FIG. 1. (a) Molecular systems used in this paper. Except for water clusters, whose structures are taken from the Cambridge Cluster Database [47], all other structures are first optimized. DME, dimethoxyethane; DOL, dioxolane; EC, ethylene carbonate; DMSO, dimethyl sulfoxide; TFSI, bis(trifluoromethanesulfonyl)imide; HQ, hydroxyquinoline. (b) Semilogarithmic plot of the time needed for serial computation (on a single CPU core) of the polarizability tensors for water clusters  $(\text{H}_2\text{O})_k$ ,  $k = 5, \dots, 20$  through LR theory relative to that required for the calculation of total covariance matrices using the WP method. Also shown (solid square) is the speedup for a bulk system containing 32 water molecules. (c)  $t_{LR}$  and  $t_{WP}$  for the same systems as functions of the number of electrons. Dashed and solid curves in red represent fits to the data points. RMSE, root-mean-square error.

the basis set size. In the WP method, however, there is no need to find the response of the system to any external perturbation. The MLWFs are calculated from the Kohn-Sham (unperturbed) orbitals followed by the estimation of their spatial extension through the covariance matrices in Eq. (4). The time needed for the latter depends mainly on the basis set size (that is, the number of electrons and the quality of the basis set) based on which the MLWFs are represented.

## B. Raman spectra of methanol in gas and liquid phases

Figure 2 shows individual elements of the polarizability tensor  $\mathbf{A}$  (red) and the total covariance matrix  $\mathbf{\Omega}$  (black) for a methanol molecule in the gas phase obtained from an AIMD trajectory of 10 000 snapshots. Diagonal elements are presented in Fig. 2(a), while off-diagonal ones are shown in Fig. 2(b). Also shown in Figs. 2(c) and 2(d) are normalized distributions of the traces,  $\text{Tr}[\mathbf{\Omega}]$  and  $\text{Tr}[\mathbf{A}]$ , and the anisotropic Raman invariants,  $\gamma_A^2$  and  $\gamma_{\Omega}^2$ . The reference polarizability tensor is again calculated using LR theory. Although the values of the polarizability tensor and the total covariance matrix elements differ substantially [Figs. 2(a) and 2(b)], there is apparently a strong correlation between them. In fact, the correlation coefficients are found to be  $\rho(\text{Tr}[\mathbf{\Omega}], \text{Tr}[\mathbf{A}]) \simeq 0.98$  and  $\rho(\gamma_{\Omega}^2, \gamma_A^2) \simeq 0.82$ . In agreement with this, the normalized distributions presented in Figs. 2(c) and 2(d) also have comparable statistical characteristics, given in Figs. 2(c) and 2(d) as insets [35].

Polarized and depolarized Raman spectra of a methanol molecule in the gas phase at 300 K are presented in Figs. 3(a) and 3(b), respectively. In the case of the WP calculations (black), the spectra are computed by replacing  $A_{ij}$  by  $\Omega_{ij}$

in Eq. (8). Other than applying a Hann window function to the time series, no other modification (for example, zero padding, local fitting, etc.) is applied to the spectra. The peak intensities in the polarized spectra [Fig. 3(a)] are scaled with respect to that of the C–H stretching peak at  $\sim 3000$  cm<sup>-1</sup>, while those in the depolarized spectra [Fig. 3(b)] are scaled with respect to rocking and scissoring vibrations of CH<sub>3</sub> at  $\sim 1500$  cm<sup>-1</sup>. The peaks at around 3000 cm<sup>-1</sup> can be assigned to symmetric and antisymmetric C–H stretching vibrations, while the Raman activities at around 1500 cm<sup>-1</sup> are due to rocking and scissoring vibrations of CH<sub>3</sub> as well as C–O–H scissoring. Finally, the peak at around 1000 cm<sup>-1</sup> can be assigned to C–O stretching. A clear difference between the spectra in Figs. 3(a) and 3(b) is the peak at around 1500 cm<sup>-1</sup> which becomes prominent in the depolarized spectra. This has to do with the fact that the rocking and scissoring of CH<sub>3</sub> as well as the C–O–H scissoring vibrations change the symmetry of the molecule more dramatically compared with the other vibrational modes. In an experimental setup for depolarized Raman spectroscopy, this would result in detection of an intensive peak at 1500 cm<sup>-1</sup> when the detector polarization is perpendicular to that of the incident laser. Note that, since the spectra corresponds to the gas phase, the observed differences between the polarized and depolarized Raman spectra should arise from molecular symmetry breaking during vibrations. Both polarized and depolarized Raman spectra calculated using the WP method agree very well with the respective reference LR spectra. However, a substantial speedup of more than 920 times is observed in the single-core computation of spectra using the WP method.

Figure 4 shows polarized [Fig. 4(a)] and depolarized [Fig. 4(b)] Raman spectra of liquid methanol computed at

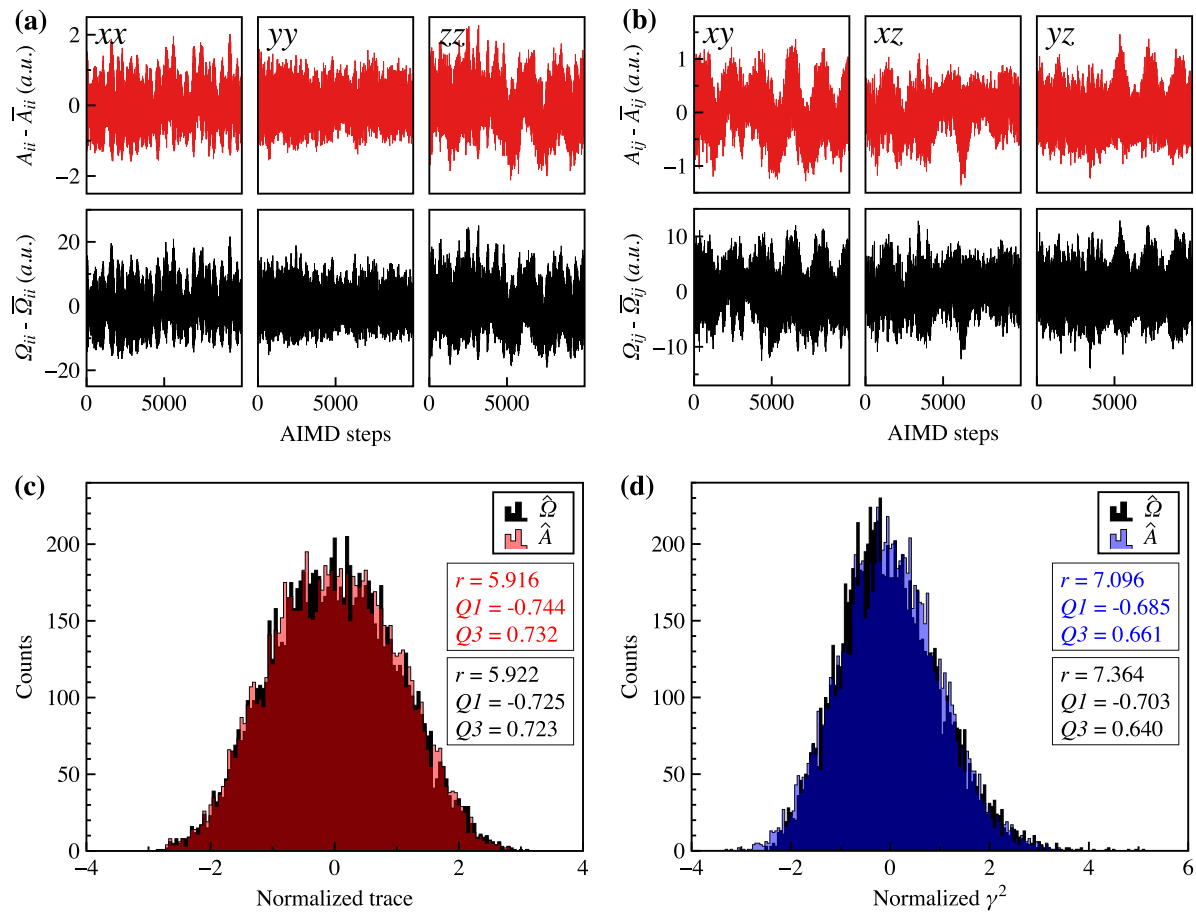


FIG. 2. (a) and (b) The dynamics of diagonal and off-diagonal elements of the polarizability tensor (red) and the total covariance matrix (black) obtained from an AIMD trajectory of a methanol molecule in the gas phase, respectively. (c) and (d) The normalized distributions of the traces,  $\text{Tr}[\hat{\Omega}]$  (black) and  $\text{Tr}[\hat{A}]$  (red), and the anisotropic Raman invariants,  $\gamma_Q^2$  (black) and  $\gamma_A^2$  (blue), respectively.

300 K using LR theory (red) and the WP method (black). In both Fig. 4(a) and Fig. 4(b) the intensities are scaled to that of the  $\text{CH}_3$  stretching vibrations at around  $3000 \text{ cm}^{-1}$ . The spectra agree very well with previous theoretical [5] and experimental [48,49] reports. The main difference between the bulk spectra and those for the gas phase is the sharp peak at around  $3700 \text{ cm}^{-1}$  in Fig. 3, which is replaced by a broad band between  $3000$  and  $3700 \text{ cm}^{-1}$  in Fig. 4. This clearly shows the effect of hydrogen bonding in liquid methanol. Additionally, both the band at  $3000 \text{ cm}^{-1}$  (C–H stretching) and the band at  $1000 \text{ cm}^{-1}$  (C–O stretching) are now broadened in the spectra of the liquid, which demonstrates the anharmonicity in these vibrations in the liquid phase at 300 K. Similar to the case gaseous methanol, the relative intensity of the C–O–H vibrations at around  $1500 \text{ cm}^{-1}$  becomes higher in the depolarized spectra, as shown in Fig. 4(b). Again, Raman spectra calculated using the WP method show a very good agreement with reference spectra computed using LR theory. A discrepancy between the WP and the LR results can, however, be detected in the intensities of the Raman peaks in the C–H stretching in the depolarized spectra.

Here a speedup of around 10 times is observed in the WP calculations compared with the computations based on

LR theory. The amounts of time needed for the LR and WP calculations are compared in Fig. 5 for the case of a methanol molecule (circles) and the case of liquid methanol (squares). Similar to the case of water [Fig. 1(c)], a scaling behavior between quadratic and cubic is observed for the calculation of MLWFs and  $\hat{\Omega}$ . This scaling behavior could be slightly improved by using alternative methods for obtaining MLWFs which are usually faster than Jacobi rotations (for example, optimal unitary transformation generated by the crazy angle algorithm). This would mostly affect the computation time in large systems where the time needed to minimize the total spread functional in Eq. (2) is comparable to that required for the calculation of covariance matrices through Eq. (4).

#### IV. CONCLUSIONS

An efficient method has been proposed to approximate the dynamics of polarizability tensor elements based on the calculation of the quadrupole moment (covariance) of the position operator in the maximally localized Wannier functions representation. It has been shown that variations of individual polarizability tensor elements during *ab initio*

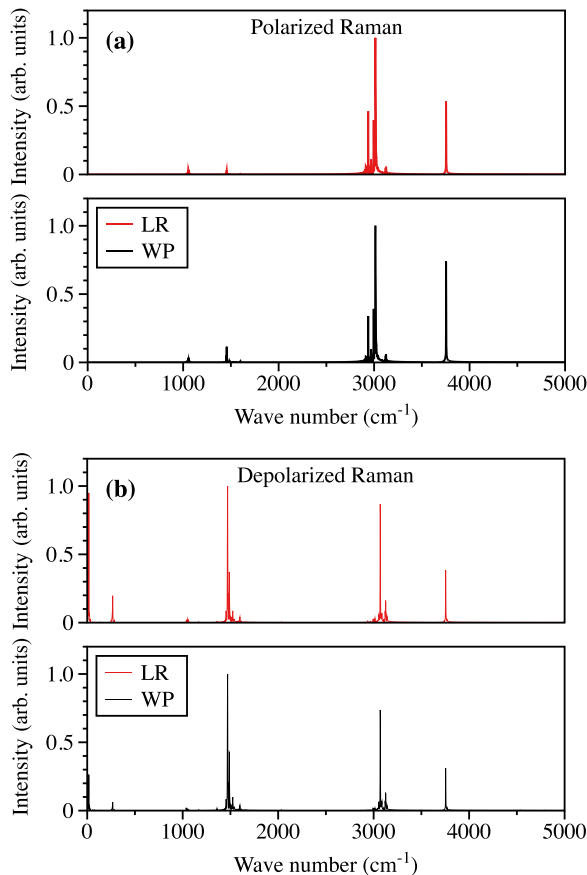


FIG. 3. Computed polarized (a) and depolarized (b) Raman spectra of gas-phase methanol at 300 K. Red and black curves represent the spectra obtained using LR theory and the WP method, respectively.

molecular dynamics simulations can be well reproduced by the total covariance matrix of Wannier centers with a significantly less computational cost. This is particularly important for spectroscopy simulations at finite temperatures where the dynamics of the full polarizability tensor is needed, such as depolarized Raman, Raman optical activity, vibrational sum-frequency generation, etc. The performance of the introduced method has been demonstrated in various cases, including gas-phase and liquid methanol. Polarized and depolarized Raman spectra of gas-phase and liquid methanol computed using the present method agree very well with reference calculations based on linear response theory. Using the presented method, a substantial speedup (based on single-core computations) of about 10 times has been reached in the case of liquid methanol modeled using a large simulation box. The speedup increases rapidly to around 140 times as the size of the simulation box is decreased. In the case of gas-phase methanol, a huge speedup of more than 900 times has been reached. Similar efficiency has also been observed in the case of water clusters. The speedup increases rapidly from about 60 times to around 1000 times as the cluster size decreases. Even in the case of extended, periodic systems, a speedup of more than 60 times has been observed in the case of liquid water. Therefore the presented method delivers the efficiency required for *ab ini-*

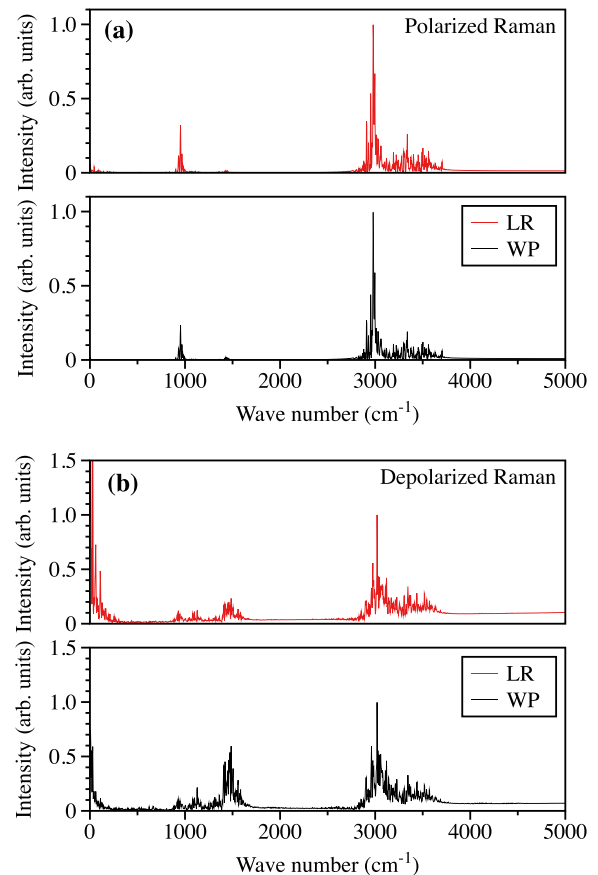


FIG. 4. Computed polarized (a) and depolarized (b) Raman spectra of liquid methanol at 300 K. Red and black curves represent the spectra obtained using LR theory and the WP method, respectively.

*to* finite-temperature spectroscopy simulations in condensed phase and hence has a wide range of applications in the theoretical characterization of materials.

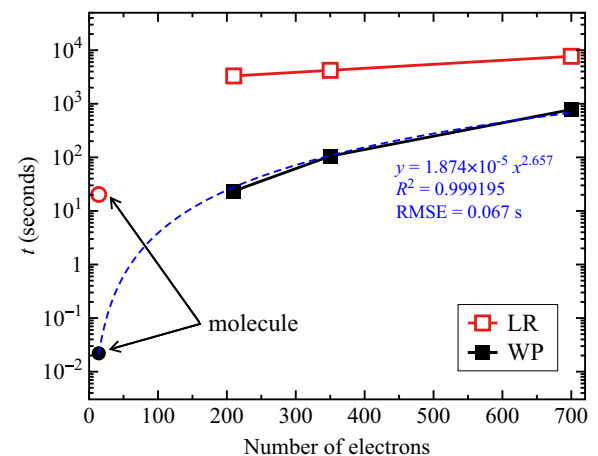


FIG. 5. Time needed for the LR (red) and WP (black) calculations for the case of a methanol molecule (circles) and the case of liquid methanol (squares) based on single-core calculations. RMSE, root-mean-square error.

## ACKNOWLEDGMENTS

The author gratefully acknowledges Deutsche Forschungsgemeinschaft funding via projects PA3141/3 (Project No. 420536636) and PA3141/5 (Project No. 446879138). The computations were performed on a Bull Cluster at the Center

for Information Services and High Performance Computing (ZIH) at TU Dresden via the project “p\_oligothiophenes.” The author also thanks Hossam Elgabarty, Daniel Sebastiani, Thomas D. Kühne, and Sara Panahian Jand for fruitful discussions.

- [1] D. A. Long, *The Raman Effect* (Wiley, New York, 2002).
- [2] A. Putrino and M. Parrinello, Anharmonic Raman spectra in high-pressure ice from *ab initio* simulations, *Phys. Rev. Lett.* **88**, 176401 (2002).
- [3] T. Ishiyama, V. V. Sokolov, and A. Morita, Molecular dynamics simulation of liquid methanol. I. Molecular modeling including C–H vibration and Fermi resonance, *J. Chem. Phys.* **134**, 024509 (2011).
- [4] T. Ishiyama, V. V. Sokolov, and A. Morita, Molecular dynamics simulation of liquid methanol. II. Unified assignment of infrared, Raman, and sum frequency generation vibrational spectra in methyl C–H stretching region, *J. Chem. Phys.* **134**, 024510 (2011).
- [5] M. Thomas, M. Brehm, R. Fligg, P. Vöhringer, and B. Kirchner, Computing vibrational spectra from *ab initio* molecular dynamics, *Phys. Chem. Chem. Phys.* **15**, 6608 (2013).
- [6] R. Khatib and M. Sulpizi, Sum frequency generation spectra from velocity–velocity correlation functions, *J. Phys. Chem. Lett.* **8**, 1310 (2017).
- [7] E. Ditler and S. Luber, Vibrational spectroscopy by means of first-principles molecular dynamics simulations, *WIREs Comput. Mol. Sci.* **12**, e1605 (2022).
- [8] H. Elgabarty, T. Kampfrath, D. J. Bonhuis, V. Balos, N. K. Kaliannan, P. Loche, R. R. Netz, M. Wolf, T. D. Kühne, and M. Sajadi, Energy transfer within the hydrogen bonding network of water following resonant terahertz excitation, *Sci. Adv.* **6**, eaay7074 (2020).
- [9] V. Balos, N. K. Kaliannan, H. Elgabarty, M. Wolf, T. D. Kühne, and M. Sajadi, Time-resolved terahertz-Raman spectroscopy reveals that cations and anions distinctly modify intermolecular interactions of water, *Nat. Chem.* **14**, 1031 (2022).
- [10] P. Partovi-Azar, T. D. Kühne, and P. Kaghazchi, Evidence for the existence of Li<sub>2</sub>S<sub>2</sub> clusters in lithium–sulfur batteries: *ab initio* Raman spectroscopy simulation, *Phys. Chem. Chem. Phys.* **17**, 22009 (2015).
- [11] P. Partovi-Azar and T. D. Kühne, Efficient “on-the-fly” calculation of Raman spectra from *ab-initio* molecular dynamics: Application to hydrophobic/hydrophilic solutes in bulk water, *J. Comput. Chem.* **36**, 2188 (2015).
- [12] Q. Wan, L. Spanu, G. A. Galli, and F. Gygi, Raman spectra of liquid water from *ab initio* molecular dynamics: vibrational signatures of charge fluctuations in the hydrogen bond network, *J. Chem. Theory Comput.* **9**, 4124 (2013).
- [13] S. Luber, M. Iannuzzi, and J. Hutter, Raman spectra from *ab initio* molecular dynamics and its application to liquid *S*-methyloxirane, *J. Chem. Phys.* **141**, 094503 (2014).
- [14] S. Luber, Sum frequency generation of acetonitrile on a rutile (110) surface from density functional theory-based molecular dynamics, *J. Phys. Chem. Lett.* **7**, 5183 (2016).
- [15] S. Luber, Raman optical activity spectra from density functional perturbation theory and density-functional-theory-based molecular dynamics, *J. Chem. Theory Comput.* **13**, 1254 (2017).
- [16] J. Mattiat and S. Luber, Vibrational (resonance) Raman optical activity with real time time dependent density functional theory, *J. Chem. Phys.* **151**, 234110 (2019).
- [17] D. Pan and G. Galli, A first principles method to determine speciation of carbonates in supercritical water, *Nat. Commun.* **11**, 421 (2020).
- [18] M. Thomas, M. Brehm, and B. Kirchner, Voronoi dipole moments for the simulation of bulk phase vibrational spectra, *Phys. Chem. Chem. Phys.* **17**, 3207 (2015).
- [19] N. Marzari and D. Vanderbilt, Maximally localized generalized Wannier functions for composite energy bands, *Phys. Rev. B* **56**, 12847 (1997).
- [20] N. Marzari, A. A. Mostofi, J. R. Yates, I. Souza, and D. Vanderbilt, Maximally localized Wannier functions: Theory and applications, *Rev. Mod. Phys.* **84**, 1419 (2012).
- [21] W. Kohn and L. J. Sham, Self-consistent equations including exchange and correlation effects, *Phys. Rev.* **140**, A1133 (1965).
- [22] P. L. Silvestrelli, N. Marzari, D. Vanderbilt, and M. Parrinello, Maximally-localized Wannier functions for disordered systems: Application to amorphous silicon, *Solid State Commun.* **107**, 7 (1998).
- [23] P. L. Silvestrelli, Maximally localized Wannier functions for simulations with supercells of general symmetry, *Phys. Rev. B* **59**, 9703 (1999).
- [24] G. Berghold, C. J. Mundy, A. H. Romero, J. Hutter, and M. Parrinello, General and efficient algorithms for obtaining maximally localized Wannier functions, *Phys. Rev. B* **61**, 10040 (2000).
- [25] P. Partovi-Azar and T. D. Kühne, Full assignment of *ab-initio* Raman spectra at finite temperatures using Wannier polarizabilities: Application to cyclohexane molecule in gas phase, *Micromachines* **12**, 1212 (2021).
- [26] R. Kiani, M. Steimecke, M. Alqaisi, M. Bron, D. Sebastiani, and P. Partovi-Azar, Characterization of sulfur/carbon copolymer cathodes for Li–S batteries: a combined experimental and *ab initio* Raman spectroscopy study, *RSC Adv.* **13**, 27756 (2023).
- [27] J. C. Bennion, P. G. Lafond, and J. A. Ciezak-Jenkins, High-pressure characterization of melt-castable bisoxazole energetics: 3,3′-bisoxazole-5,5′-bis-(methylene) dinitrate and 3,3′-bisoxazole-4,4′, 5,5′-tetrakis-(methylene nitrate), *Propellants Explos. Pyrotech.* **44**, 1015 (2019).
- [28] R. F. Bader, Atoms in molecules, *Acc. Chem. Res.* **18**, 9 (1985).
- [29] K. Gough, Theoretical analysis of molecular polarizabilities and polarizability derivatives in hydrocarbons, *J. Chem. Phys.* **91**, 2424 (1989).
- [30] K. E. Laidig and R. F. Bader, Properties of atoms in molecules: Atomic polarizabilities, *J. Chem. Phys.* **93**, 7213 (1990).

- [31] T. Brinck, J. S. Murray, and P. Politzer, Polarizability and volume, *J. Chem. Phys.* **98**, 4305 (1993).
- [32] W. A. Wheeler, L. K. Wagner, and T. L. Hughes, Many-body electric multipole operators in extended systems, *Phys. Rev. B* **100**, 245135 (2019).
- [33] B. Kang, K. Shiozaki, and G. Y. Cho, Many-body order parameters for multipoles in solids, *Phys. Rev. B* **100**, 245134 (2019).
- [34] R. Resta, Quantum-mechanical position operator in extended systems, *Phys. Rev. Lett.* **80**, 1800 (1998).
- [35] See Supplemental Material at <http://link.aps.org/supplemental/10.1103/PhysRevB.108.235157> for the effect of cross correlations in Raman spectroscopy simulations using the WP method, as well as cumulative probabilities and the Kolmogorov-Smirnov test for  $\text{Tr}[\mathbf{A}]$ ,  $\text{Tr}[\mathbf{\Omega}]$ ,  $\gamma_A^2$ , and  $\gamma_{\mathbf{\Omega}}^2$ , together with remarks on the timing calculations.
- [36] S. Mukamel, *Principles of Nonlinear Optical Spectroscopy*, Oxford Series in Optical and Imaging Sciences (Oxford University Press, New York, 1995).
- [37] R. Ramírez, T. Lopez-Ciudad, P. Kumar P, and D. Marx, Quantum corrections to classical time-correlation functions: Hydrogen bonding and anharmonic floppy modes, *J. Chem. Phys.* **121**, 3973 (2004).
- [38] P. Polavarapu, L. Hecht, and L. Barron, Vibrational Raman optical activity in substituted oxiranes, *J. Phys. Chem.* **97**, 1793 (1993).
- [39] T. D. Kühne, M. Iannuzzi, M. Del Ben, V. V. Rybkin, P. Seewald, F. Stein, T. Laino, R. Z. Khaliullin, O. Schütt, F. Schiffmann, D. Golze, J. Wilhelm, S. Chulkov, M. H. Bani-Hashemian, V. Weber, U. Borštnik, M. Taillefumier, A. S. Jakobovits, A. Lazzaro, H. Pabst *et al.*, CP2K: An electronic structure and molecular dynamics software package - Quickstep: Efficient and accurate electronic structure calculations, *J. Chem. Phys.* **152**, 194103 (2020).
- [40] J. Vandevondele and J. Hutter, Gaussian basis sets for accurate calculations on molecular systems in gas and condensed phases, *J. Chem. Phys.* **127**, 114105 (2007).
- [41] A. D. Becke, Density-functional exchange-energy approximation with correct asymptotic behavior, *Phys. Rev. A* **38**, 3098 (1988).
- [42] C. Lee, W. Yang, and R. G. Parr, Development of the Colle-Salvetti correlation-energy formula into a functional of the electron density, *Phys. Rev. B* **37**, 785 (1988).
- [43] S. Goedecker, M. Teter, and J. Hutter, Separable dual-space Gaussian pseudopotentials, *Phys. Rev. B* **54**, 1703 (1996).
- [44] M. Krack, Pseudopotentials for H to Kr optimized for gradient-corrected exchange-correlation functionals, *Theor. Chem. Acc.* **114**, 145 (2005).
- [45] S. Grimme, J. Antony, S. Ehrlich, and H. Krieg, A consistent and accurate *ab initio* parametrization of density functional dispersion correction (DFT-D) for the 94 elements H-Pu, *J. Chem. Phys.* **132**, 154104 (2010).
- [46] G. Bussi, D. Donadio, and M. Parrinello, Canonical sampling through velocity rescaling, *J. Chem. Phys.* **126**, 014101 (2007).
- [47] S. Maheshwary, N. Patel, N. Sathyamurthy, A. D. Kulkarni, and S. R. Gadre, Structure and stability of water clusters  $(\text{H}_2\text{O})_n$ ,  $n = 8-20$ : An *ab initio* investigation, *J. Phys. Chem. A* **105**, 10525 (2001).
- [48] Y. Yu, Y. Wang, K. Lin, N. Hu, X. Zhou, and S. Liu, Complete Raman spectral assignment of methanol in the C-H stretching region, *J. Phys. Chem. A* **117**, 4377 (2013).
- [49] spectraBase Compound ID=CyEzolQHtsY SpectraBase Spectrum ID=FQ2skpdfLUw, in *SpectraBase* (Wiley, New York, 2023), <https://spectrabase.com/spectrum/FQ2skpdfLUw>.